Article

Combined In Situ and In Silico Studies of Guest Intercalation into the Layered Double Hydroxide [LiAl2(OH)6]X•yH2O

Abdessamad Yacine Kaassis, Simin Xu, David G. Evans, Min Wei, Gareth R. Williams, and Xue Duan

Just Accepted

1
2
3
4
5
6
7
8
9
10
11
12
13
14
15
16
17
18
19
20
21
22
23
24
25
26
27
28
29
30
31
32
33
34
35
36
37
38
39
40
41
42
43
44
45
46
47
48
49
50
51
52
53
54
55
56
57
58
59
60

Combined *In Situ* and *In Silico* Studies of Guest Intercalation into the

Layered Double Hydroxide [LiAl$_2$(OH)$_6$]X·yH$_2$O

Abdessamad Y A. Kaassis,[a] Si-Min Xu,[b] David G. Evans,[b] Gareth R. Williams,[a]* Min Wei,[b]* and Xue Duan[b]

a   UCL School of Pharmacy, University College London, 29-39 Brunswick Square, London, WC1N 1AX, UK.

b   State Key Laboratory of Chemical Resource Engineering, Beijing University of Chemical Technology, Beijing 100029, P. R. China

* authors for correspondence. Email: weimin@mail.buct.edu.cn (MW); g.williams@ucl.ac.uk (GRW); Tel: +86 (0)106 441 2131 (MW): +44 (0)207 753 5868 (GRW).

Abstract

Phosphonoacetate (PAA), diethyl phosphonoacetate (DPA) and sulfoacetate (SAA) anions have been intercalated into the galleries of the layered double hydroxide (LDH) $[LiAl_2(OH)_6.X]\cdot yH_2O$ (LiAl-X; X = Cl, NO_3). X-ray diffraction (XRD), Fourier transform infrared spectroscopy, and elemental microanalysis confirmed the successful intercalation of the guest ions into the LDH. The guests could all be recovered from the host intact. *In situ* XRD was used to probe the mechanisms of the reactions, and the intercalation of PAA proceeded *via* clear intermediate phases. In contrast, the SAA and DPA reactions did not show any intermediates, but the organic intercalates exhibited changes in their interlayer spacing as the reaction progressed. Molecular dynamics (MD) simulations were used to investigate the interlayer structure and orientation of the intercalation compounds. It was found that the intermediates observed *in situ* correspond to local energy minima in the MD simulations. MD can thus predict the course of an intercalation reaction, and allow the *a priori* identification of intermediate phases. This is the first time that *in silico* and *in situ* measurements have been used to unravel this level of understanding of intercalation reactions.

Keywords

LDH; time-resolved X-ray diffraction; molecular dynamics; reaction intermediate

Introduction:

Layered double hydroxides (LDHs), also known as hydrotalcite-like compounds, are a widely-studied class of ion exchange materials. They consist of positively charged metal hydroxide sheets and charge balancing anions in the interlayer region. The general formula of LDHs is $[M^z_{1-x}M^{3+}_x(OH)_2]^{q+}(X^{n-})_{q/n}\cdot yH_2O$. Generally $z=2$, and M^{2+} is a divalent metal such as Mg, Co, Ni, Cu, Zn or Ca; M^{3+} is a trivalent metal such as Al. There is also a unique family of LDHs for which $z = 1$, where $M^+ = Li^+$ and $q = 2x - 1$. The common formula for this family of materials is $[LiAl_2(OH)_6]X\cdot yH_2O$ (LiAl-X), where y lies in the approximate range $0.5 - 4$ and X is a generic anion (*e.g.* Cl, Br, and NO_3). [1] This family of materials is known to exist in hexagonal (2H) and rhombohedral (3R) polytypes; these differ in their layer stacking sequences, with 2H materials having a two-layer repeat *aba* stacking sequence and 3R possessing a three-layer *abca* repeat. [2] The layers stack in the c-direction, which means that a 2H unit cell contains two layers and a 3R cell has three.

Interest in LDHs has increased in recent years because of their utility as flame retardants,[3] catalysts and catalyst precursors,[4–6] water and air purifying agents,[7,8] adsorbents,[9–11] electrical and optical functional materials,[12] and for the separation of organic isomers.[13,14] They have also been shown to have potential as drug delivery systems,[15,16] and for the stabilisation of pharmaceutical salts of antipyretic, analgesic and anti-inflammatory drugs.[17] A range of organic species featuring different functional groups including carboxylates,[15,18–211-4] phosphonate,[22–26] and sulfonates[21,27–29] have been intercalated.

Although the intercalation of an enormously wide range of species into LDHs has been reported, the precise nanoscopic processes which take place during guest uptake remain poorly understood. This is in part because the most accessible method to obtain such insight, quenching the reaction, is invasive and known potentially to affect the outcome of the reaction. To gain reliable understanding of solid-state reaction processes, a non-invasive probe is required. Few such probes exist, but the technique of time-resolved *in situ* diffraction using a synchrotron X-ray source is one which permits us to obtain detailed information on solid state

or solid/liquid reaction processes without affecting the course of the reaction. It has been used to great effect to begin to unravel the kinetics and mechanisms of intercalation processes.[30]

Time resolved X-ray diffraction (XRD) has been used to probe a range of LDH intercalation reactions; particularly interesting results have been obtained for the incorporation of carboxylate and phosphonate species. The intercalation of such species into the LiAl-X family of LDHs has revealed that the reactions in some cases proceed *via* so-called "second stage" intermediates, in which alternate interlayer spaces are occupied by the starting anion X and the incoming ion. [24,31,32] Whether the reaction proceeds directly from the host to the product or *via* a second stage intermediate has been shown to be dependent on the incoming ion, the layer stacking sequence of the LDH (*aba* hexagonal, or *abca* rhombohedral),[33] the initial interlayer ion,[33] the reaction temperature,[26] and the solvent system.[26] It has also been shown that if the second stage phases can be isolated, then they exhibit selective ion exchange properties, with (in)organic guests preferentially replaced by other (in)organics.[34]

In this work, we sought to build on the earlier work exploring phosphonates and carboxylates, and investigated the intercalation of three bifunctional ions (phosphonoacetic acid, sulfoacetic acid, and diethylphosphonoacetic acid) into the hexagonal LiAl-Cl and LiAl-NO$_3$ LDH systems. These systems were selected because for organic phosphonates and carboxylates second stage intermediates have been reported to occur for the hexagonal form of LiAl-Cl, but not for its nitrate analogue. The final products obtained after incorporation of the bifunctional anions into the [LiAl$_2$(OH)$_6$]X·H$_2$O system were first synthesised and fully characterised. A range of *in situ* diffraction experiments were then used to probe the intercalation mechanisms. We coupled the use of *in situ* diffraction techniques with molecular dynamics (MD) simulations to provide additional insight into the phase transformations observed. MD is a valuable tool for complementing experimental work in terms of understanding of the interactions between the LDH layer and the guest ions. The technique allows the interlayer arrangements and dynamics of guest ions and water molecules to be evaluated. There have been several MD studies of LDH

intercalates, for instance of amino-acids,[35] benzocarbazole,[36] lanthanide complexes,[37] organic luminescent materials,[38–40] and even DNA.[41,42]

Materials and methods

Materials

Lithium chloride; lithium nitrate, phosphonoacetic acid (PAA), sulfoacetic acid (SAA), and diethyl phosphonoacetic acid (DPA) were purchased from Sigma Aldrich (UK). Gibbsite (γ-Al(OH)$_3$) was a kind gift from Prof Dermot O'Hare of Oxford University. All chemicals were of analytical grade and used without further purification.

LDH synthesis

The hexagonal polymorph of [LiAl$_2$(OH)$_6$]Cl·yH$_2$O (LiAl-Cl) was synthesised using methods reported previously.[43] In a standard experiment, 1g of γ-Al(OH)$_3$ was combined with a 6-fold molar excess of LiCl in 10mL deionised water. The reaction mixture was stirred and heated at 90 °C for *ca.* 48 h in a sealed ampoule. The solid product was recovered by vacuum filtration, washed with copious amounts of deionised water, a small amount of acetone, and then allowed to dry under vacuum. The hexagonal form of [LiAl$_2$(OH)$_6$]NO$_3$·yH$_2$O (LiAl-NO$_3$) was prepared using analogous procedures but with LiNO$_3$ in place of LiCl.

Intercalation reactions

Three different PAA species were prepared by reacting one equivalent of PAA with 1, 2 or 3 equivalents of NaOH; these are respectively denoted PAA$^-$, PAA^{2-} and PAA^{3-}. Intercalation was achieved by combining 0.2 mmol of LiAl-Cl (or LiAl-NO$_3$) with a 2-fold excess of the guest. The LDH was added to 10 mL of a 40 mM guest solution, and the mixture stirred at room temperature for a pre-determined period of time (1h – 24h). The solid products were recovered by vacuum filtration, washed, and dried. SAA and DPA were intercalated in an analogous manner: DPA was combined with 1 equivalent of NaOH and SAA with 2 equivalents of NaOH, before a two-fold excess of the ions was reacted with the LDH. The final products are denoted LiAl-X, where X = PAA^{3-}, PAA^{2-}, PAA$^-$, SAA or DPA.

Guest recovery

The ability to recover the guest ions intact after intercalation was investigated in selected cases by reacting *ca.* 50 mg of the intercalate with approximately 100 mg of Na_2CO_3 in D_2O overnight at 80 °C. The resultant suspension was filtered and the filtrate analysed by ^{1}H NMR.

Characterisation

X-ray diffraction

X-ray diffraction (XRD) was performed using a Philips PW1830 instrument operating at 40 kV and 25 mA with Cu Ka radiation (λ = 1.5418 Å). Samples were finely ground (using a mortar and pestle) and mounted on aluminium plates for measurement. Diffracted intensity from the sample holder did not interfere with sample characterisation.

IR spectroscopy

IR spectra were recorded on a Perkin Elmer Spectrum 100 instrument. Data were recorded from 4000 to 650 cm^{-1} at a resolution of 2 cm^{-1}.

NMR spectroscopy:

^{1}H NMR spectra were obtained on a Bruker Avance-400 instrument at ambient temperature (1H frequency: 400 MHz).Samples were dissolved in D_2O prior to measurement.

Elemental analysis

C, H, and N contents were determined using the quantitative combustion technique on a Carlo Erba CE1108 elemental analyser.

Thermogravimetric analysis

Thermogravimetric analysis (TGA) was performed on a Discovery analyser (TA Instruments). *Ca.* 3 – 4 mg of each sample was weighed into an aluminium pan and heated at a rate of 10 $^{\circ}C$ min^{-1} from room temperature to 400 $^{\circ}C$ under an N_2 flux (10 mL min^{-1}).

In situ **X-ray diffraction**

The first series of i*n situ* energy-dispersive X-ray diffraction (EDXRD) measurements was performed on Beamline F3 of the DORIS synchrotron at the Deutsches Elektronen-Synchrotron (DESY), Hamburg, Germany. The beamline is supplied with a white-beam of X-rays over the energy range 13.5 to 65 keV. Reactions were performed in borosilicate glass vessels using a purpose built furnace system; details of the apparatus used are given elsewhere.[24] *In situ* XRD was also undertaken at the Diamond Light Source, using Beamline I12. For these experiments, the X-ray beam was monochromated to *ca.* 53 keV, and data collected with a Thales Pixium RF4343 detector positioned 2 m from the reaction vessel. Experiments on I12 were conducted in glassy carbon tubes with the aid of the Oxford-Diamond *In Situ* Cell (ODISC).[44]

Both at DESY and on I12, 0.4 mmol of the desired LDH was suspended under stirring in 5 mL of deionised water, and 10 mL of a solution containing 0.8 mmol of the guest ion was added dropwise using a syringe pump (KDS100, Cole-Parmer). Diffraction patterns were recorded every 60 seconds (DESY) or 4 seconds (Diamond) until no further changes in these were observed. Data analysis was performed by integrating reflections of interest using the F3Tool software (DESY), or by employing Fit2D[45] to convert the as-collected images into one-dimensional patterns, subtracting the background, and applying in-house tools to integrate the reflections of interest (Diamond). Integrated data were subsequently probed using the Avrami–Erofe'ev model;[46–49] more details are given in the results section.

Modelling

Models of the LiAl LDH systems were built in the space group P6$_3$/m, using the structure previously reported by O'Hare *et. al.*[43] In this symmetry, $\alpha = \beta = 90°$, $\gamma = 120°$. The molar ratio of Li$^+$ to Al^{3+} is 1:2. The formulae of these five models are listed in Table 1. All MD simulations were performed adopting the LDHFF force field developed by Zhang *et al.* in an isothermal-isobaric (NPT) ensemble.[50] Temperature and pressure control were performed using the Andersen method[51] and the Berendsen method,[52] respectively. Long-range Coulombic interactions were computed by the Ewald summation technique [53] and van der Waals

interactions using a "spline-cut off" method. The time-step was set to be 1 fs, which is suitable for the characterisation of thermal motion,[54] and the simulation time was 5 ns. All MD simulations were carried out using the Forcite module in the Materials Studio v5.5 software package (Accelrys Software Inc, San Diego, CA, USA).[55]

Table 1: The formulae of the LiAl LDH models used for molecular dynamics work.

Material	Formula for constrained model	Formula for unconstrained model
LiAl-PAA^{3-}	$[LiAl_2(OH)_6]_{12}(C_2PO_5H_2)_4 \cdot 12H_2O$	$[LiAl_2(OH)_6]_{10}(C_2PO_5H_2)_2(C_2PO_5H_3)_2 \cdot 12H_2O$
LiAl-PAA$^-$	$[LiAl_2(OH)_6]_{12}(C_2PO_5H_4)_{12} \cdot 12H_2O$	$[LiAl_2(OH)_6]_6(C_2PO_5H_4)_6 \cdot 9H_2O$
LiAl-SAA	$[LiAl_2(OH)_6]_8(C_2SO_5H_2)_4 \cdot 8H_2O$	$[LiAl_2(OH)_6]_4(C_2SO_5H_2)_2 \cdot 4H_2O$
LiAl-DPA	$[LiAl_2(OH)_6]_8(C_6PO_5H_{12})_8 \cdot 16H_2O$	$[LiAl_2(OH)_6]_4(C_6PO_5H_{12})_4 \cdot 8H_2O$

Results and discussion

Intercalation

X-ray diffraction

Successful PAA intercalation was clearly evidenced by X-ray diffraction (XRD), IR spectroscopy, and elemental microanalysis. The XRD patterns of the reaction products (Figure 1) do not show any of the characteristic basal reflections of the starting material, and the (00l) basal reflections are observed to shift to lower angle. This corresponds to an increase in interlayer spacing, implying the incorporation of a larger anion. The intercalation of the three different PAA anions into LDHs thus appears to have been successful.
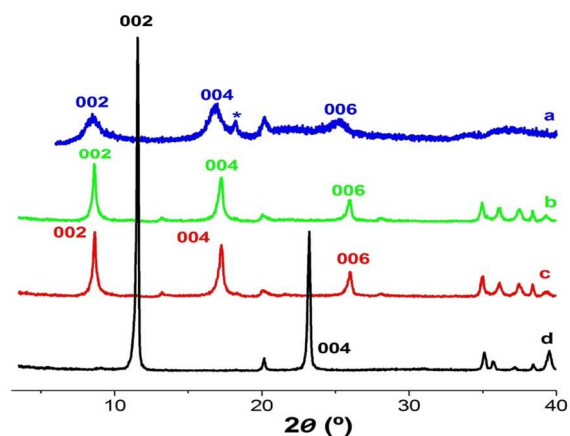
Figure 1: XRD patterns of **(a)** LiAl-PAA⁻, **(b)** LiAl-PAA^{2-}, **(c)** LiAl-PAA^{3-} and **(d)** the LiAl-Cl starting material. The reflection marked * corresponds to gibbsite [γ-Al(OH)$_3$].

The LiAl-PAA⁻ material shows a slightly higher interspacing (11.1 Å) than the PAA^{2-} and PAA^{3-} intercalates (for which d$_{002}$ is 10.2 Å). There also appears to be a small reflection attributable to gibbsite in the pattern of LiAl-PAA⁻ and the overall crystallinity is much reduced, with broadened reflections clearly notable. We cannot be certain why this arises, but we believe it to be a result of the low pH (2.5) of the PAA⁻ solution causing some degradation of the sample. In addition, the lower charge density of the monoanionic guest may encourage turbostratic disorder in the material. A simple comparison of the interlayer spacings of the three PAA intercalates with the length of the molecules (calculated with Marvin),[56] suggests that the guests are aligned in a monolayer with their long axes perpendicular to the LDH layers. A summary of the data collected on the intercalates is presented in Table 1. It appears that when two and three equivalents of NaOH are used to ionise PAA, a mixture of mono- and di- or di- and tri-anionic species are intercalated; this is sensible given that there will be an equilibrium between these species existing in solution. The materials prepared from LiAl-Cl and LiAl-NO$_3$ are virtually identical.

As for the PAA systems, the XRD patterns of LiAl-SAA and LiAl-DPA show (002) reflections at lower angle than the starting material, confirming successful intercalation (Supporting Information, Figure S1). The DPA intercalate is poorly crystalline, and with the SAA-containing material it appears that a small amount of unreacted starting material is present alongside the

product. On the basis of guest size and interlayer spacing comparisons, it is thought that the SAA anions adopt a perpendicular monolayer arrangement while the DPA guests are organised in a perpendicular bilayer arrangement in the interlayer space, with carboxylate groups facing the positively charged layers and diethyl groups in the centre of the interlayer region. Characterising data may be found in Table 2.

Table 2: A summary of key characterising data on the intercalated phases of LiAl$_2$-X.

| ID | d_{002} / Å | | Formula[a] | Elemental analysis / % Obsd (calcd)[b] |
	X = Cl	X = NO$_3$		
LiAl-X	7.65	8.95	$[LiAl_2(OH)_6]X \cdot yH_2O$	
LiAl-PAA$^-$	11.1	11.0	$[Li_{0.8}Al_2(OH)_6](PO_3HCH_2CO_2H)_{0.8} \cdot 1.75H_2O$	C 5.73 (6.32) H 3.81 (4.21) H$_2$O 10.1 (10.4)
LiAl PAA^{2-}	10.2	10.4	$[Li_{0.95}Al_2(OH)_6](PO_3CH_2CO_2H)_{0.4}(PO_3HCH_2CO_2H)_{0.15} \cdot 2.0H_2O$	C 5.02 (4.81) H 4.46 (4.22) H$_2$O 11.5 (13.1)
LiAl-PAA^{3-}	10.2	10.2	$[Li_{0.96}Al_2(OH)_6](PO_3CH_2CO_2H)_{0.3}(PO_3CH_2CO_2)_{0.12} \cdot 1.5H_2O$	C 4.23 (4.08) H 4.28 (4.13) H$_2$O 10.5 (10.9)
LiAl-SAA	10.5	10.7	c	c
LiAl-DPA	18.6	19.2	$[Li_{0.9}Al_2(OH)_6](PO_3(C_2H_5)_2CH_2CO_2)_{0.4}Cl_{0.5} \cdot 2.5H_2O$	C 9.00 (9.51) H 4.71 (5.25) H$_2$O 11.2 (14.9)

[a] Determined for the samples prepared from LiAl-Cl.
[b] C and H contents were determined by quantitative combustion, and the H$_2$O content from TGA.
[c] It proved impossible to analyse the LiAl-SAA material by quantitative combustion.

IR spectroscopy

Selected IR spectra are given in Figure 2. LiAl-Cl shows a broad band due to the H-bonded OH groups of the LDH layer (centred at *ca.* 3400 cm^{-1}), and an absorption at around 1640 cm^{-1} as a result of the δ-bend of interlayer water molecules. PAA^{2-} has carboxylate bands between 1380 and 1570 cm^{-1} and phosphate bands at 900 – 1250 cm^{-1}. Its intercalation compound LiAl-PAA^{2-} exhibits all of these features, indicating successful intercalation of the intact guest. The spectra of the other intercalation compounds similarly exhibit the characteristic bands from their guest ions: in all cases successful intercalation is confirmed by IR spectroscopy (data for DPA, PAA$^-$ and PAA^{3-} may be found in Figures S2 and S3).
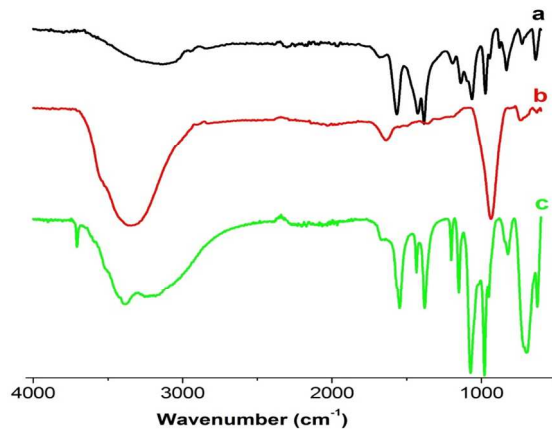
Figure 2: The FTIR spectra of **(a)** PAA^{2-}, **(b)** LiAl-Cl, and **(c)** LiAl-PAA^{2-}.

Guest recovery

Selected LiAl-PAA intercalates were reacted with Na$_2$CO$_3$ in D$_2$O, and NMR spectra recorded of the filtrate from these reactions. The spectra after deintercalation are observed to be identical to those of the PAA starting material, confirming that the structural integrity of the drug molecule is retained (data not shown).

The intercalation process

The intercalation of phosphonate and dicarboxylate guests has previously been shown to be interesting mechanistically, with second stage intermediates having been reported.[24,26,32–34] Experiments were thus performed to study the reaction of the PAA, SAA, and DPA anions with LiAl-Cl and LiAl-NO$_3$, with the intent of developing more understanding of the reaction mechanisms.

The intercalation of all three PAA anions was found to be very rapid, even at room temperature, and thus the reactions could not be followed satisfactorily. This has previously been reported by O'Hare and co-workers for similar systems.[24,32] In order to obtain mechanistic information, solutions of the PAA ions were added dropwise to aqueous suspensions of the LDH materials. Intercalation was studied at room temperature, and in some cases also with the LDH suspension heated to 70 °C.

Intercalation of PAA^{3-}

In situ diffraction data for the intercalation of PAA^{3-} are given in Figure 3. At both RT and 70 °C, a crystalline intermediate phase was observed in the diffraction data. This possesses a higher d-spacing than the final LiAl-PAA^{3-} product. It is clear from the raw experimental data given in Figure 3(a) and (b) that the intermediate and product appear at the same d-spacing regardless of which LDH starting material (LiAl-Cl or LiAl-NO$_3$) is used. The intensities of the LiAl-Cl and LiAl-PAA^{3-} (002) reflections and the intermediate reflection were integrated for each reaction, and converted to the extent of reaction, α:

$$\alpha = I_{hkl}(t)/I_{hkl}(max) \tag{1}$$

where $I_{hkl}(t)$ is the intensity of a reflection hkl at time t, and $I_{hkl}(max)$ is the maximum intensity of that reflection. Plots of α *vs.* time for intercalation into LiAl-Cl and LiAl-NO$_3$ are depicted in Figure 3(c) and (d). The α *vs.* t curves of the starting material and final product cross close to α = 0, which confirms the presence of an intermediate phase. This crossing point indicates that the loss of diffracted intensity from the starting material is complete before any product reflections grow into the system. If there was not an intermediate phase, the curves should cross near α = 0.5. The LiAl-Cl/intermediate and intermediate/LiAl-PAA^{3-} curves both cross at α = 0.5, however, indicating that there are no additional phases present on the reaction coordinate.

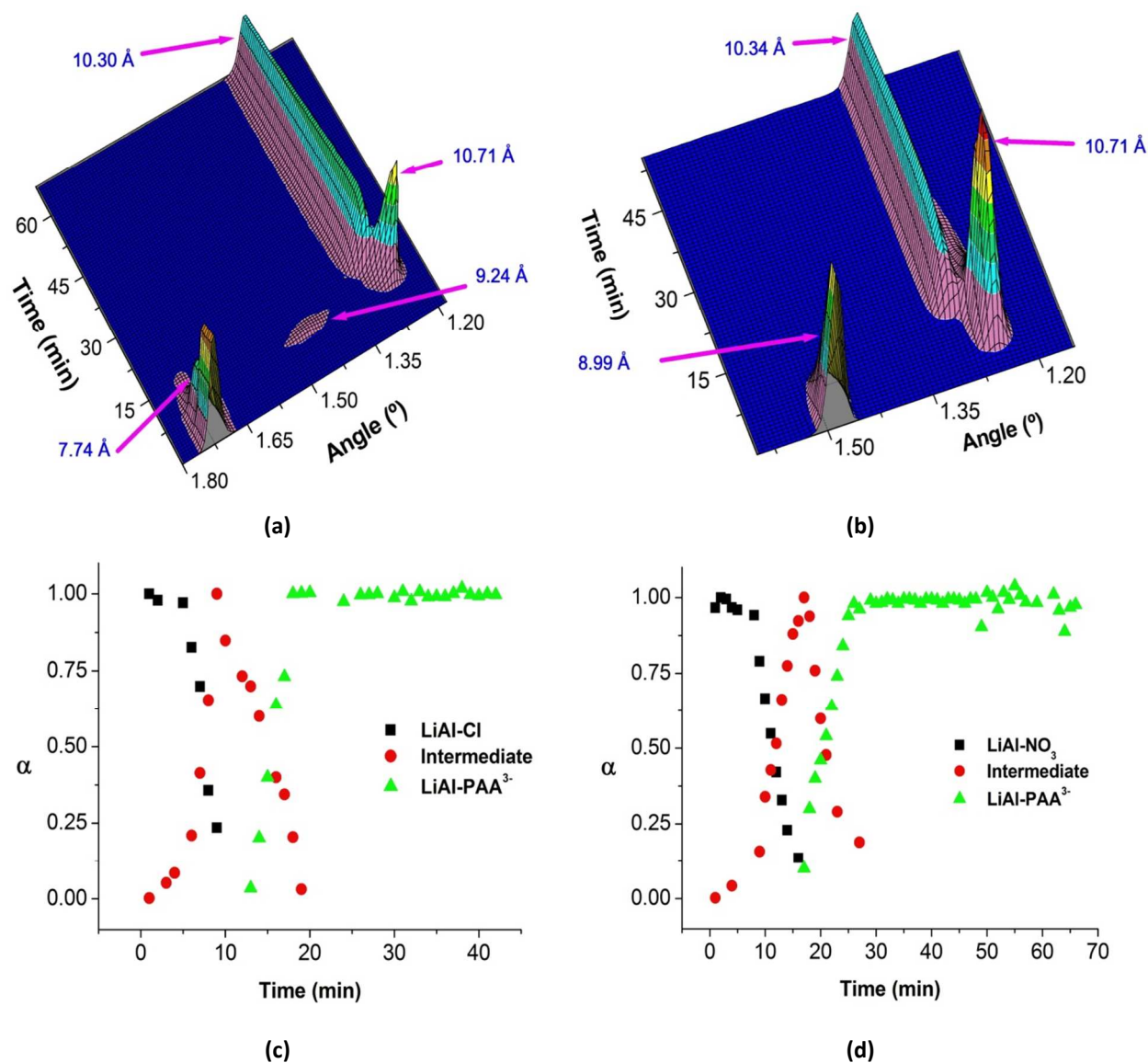**Figure 3:** *In situ* XRD data for the intercalation of PAA^{3-} into LiAl-Cl and LiAl-NO$_3$. 3D stacked plots of the raw data obtained at Diamond are given for **(a)** LiAl-Cl and **(b)** LiAl-NO$_3$, together with α *vs.* time plots for **(c)** LiAl-Cl and **(d)** LiAl-NO$_3$.

Experiments were performed both at Diamond and DESY to ensure the reproducibility of the results obtained (data from DESY are not shown in the interests of brevity). In Figure 3(a), a small reflection can be seen at 9.24 Å in the data for LiAl-Cl. This was not observed when the same experiment was performed at DESY, but a quenching experiment suggested that this is likely to be a real phase rather than an artefact, and thus we believe that this reflection may

correspond to an additional, very transient, intermediate phase (see Figure S4). The reflection at 9.24 Å is rather broad, typical of the very early stages of intercalation where some galleries contain PAA^{3-} ions and others do not. It is uncertain why this is not observed with the nitrate system, but this could be a result of overlap with the $LiAl-NO_3$ starting material (002) reflection.

Second stage intermediates have previously been observed by O'Hare and co-workers for the intercalation of both organic phosphonates and carboxylates into $LiAl-Cl$,[24,32,33] but in this case it does not appear that the intermediates correspond to staged systems. The d_{002} value expected for a second stage intermediate of PAA^{3-} and $LiAl-Cl$ would be $[d_{002}(LiAl-Cl) + d_{002}(LiAl-PAA^{3-})] =$ 17.9 Å (probably too high to be observed using the experimental configuration used), giving d_{004} of 8.97 Å. For a third stage system d_{002} should be 25.7 Å, and $d_{004} = 12.8$ Å. For $LiAl-NO_3$, the equivalent d_{004} spacings would be 9.58 and 14.1 Å respectively. The major intermediate observed experimentally has a reflection at 10.71 Å, very different to those expected for a staged system. Staging is further ruled out when quenching studies were undertaken: no very low-angle reflections indicating the presence of a supercell were observed (see Figures S4 and S5). Finally, use of both the chloride and nitrate starting materials results in the same intermediate, and thus staging cannot be operational (if it was, the intermediates should have different reflection positions).

To understand more about the intercalation process, a series of molecular dynamics (MD) simulations were undertaken (Figure 4) on the Cl-derived systems. The model was set-up using one water molecule per Li^+ ion and the interlayer spacing determined experimentally (the "constrained model"; see Tables 1 and 2).
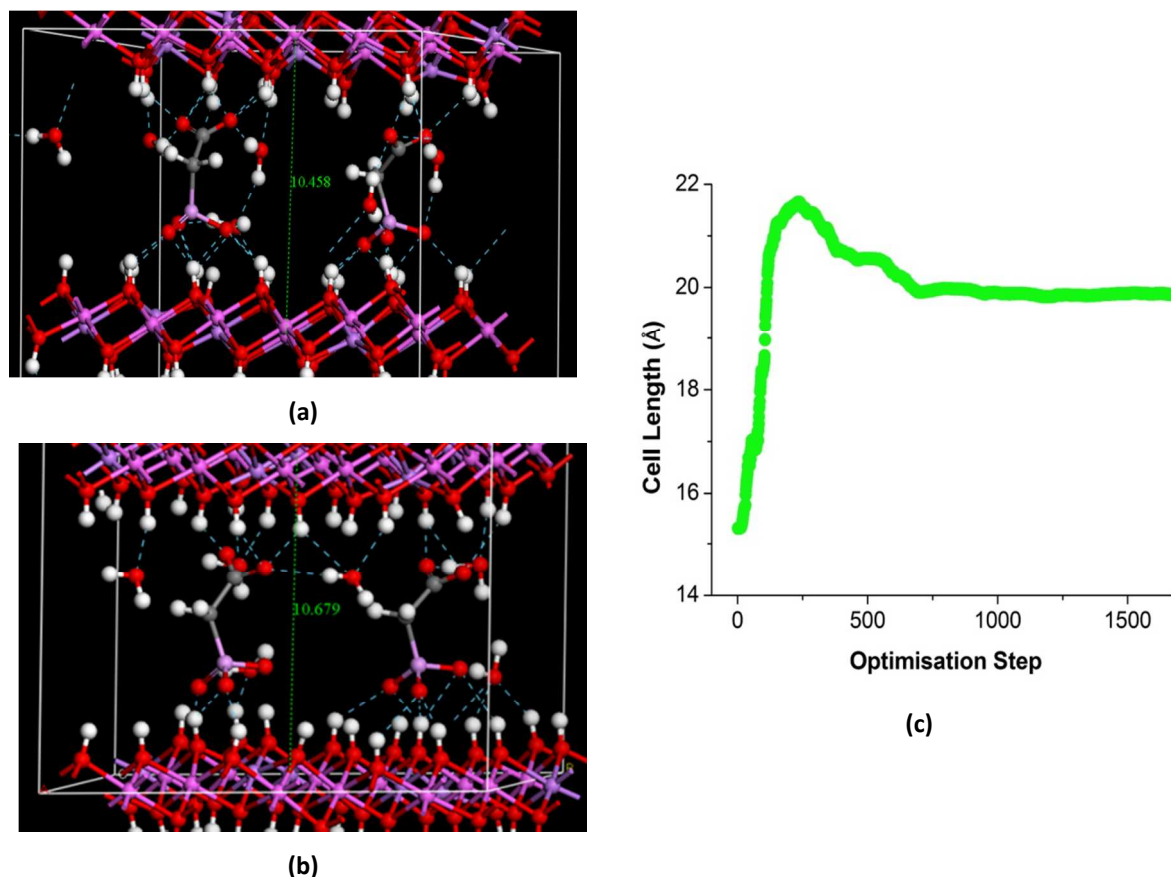
Figure 4: MD results for the intercalation of PAA[3-] into LiAl-Cl. **(a)** the orientation of PAA[3-] in the interlayer space of the energy minimised structure, **(b)** the orientation of PAA[3-] in the intermediate phase, and, **(c)** the change in the unit cell c-parameter with optimisation step.

First, we allowed the simulation to run until the energy of the system was minimised. This resulted in the model given in Figure 4(a). The PAA[3-] ions can be seen to form a monolayer, resulting in an interlayer spacing of 10.45 ± 0.04 Å (the PAA[3-] atomic positions are reported in Table S1). This result is in good agreement with the experimental values both *ex situ* and *in situ* (10.2 and 10.3 Å), with the small difference between experimental and simulation being well within the range of deviations reported in previous LDH modelling studies.[35,57–60] The PAA[3-] ions adopt an almost perpendicular position, lying across the interlayer region to interact with two adjacent layers through H-bonding. We also modelled the orientation of the ions in the major intermediate phase, feeding the d_{002} value observed for this into the model. The arrangement

of molecules here is similar to the final product (see Figure 4(b)), but there are subtle differences in the orientation of the PAA^{3-} ions.

Next, we explored the simulation process in more detail, and plotted the change in cell c-parameter as a function of the optimisation cycle number (Figure 4(c)). This experiment was undertaken by reading the known structure for $[LiAl_2(OH)_6]Cl \cdot H_2O$ into Materials Studio, deleting the Cl ions, and manually inserting PAA^{3-} between the layers. The PAA^{3-} ions were inserted in the configuration which gave the lowest energy when the c-parameter was fixed at 15.3 Å. This model (the "unconstrained model") was then allowed to optimise without constraints. Remarkably, it can be seen that the changes in c-parameter observed track very closely what is observed *in situ*: the c-parameter increases from 15.3 Å (d_{002} = 7.65 Å) in the first optimisation step to 21.6 Å (d_{002} = 10.8 Å), where it remains at a plateau for a number of optimisation cycles (presumably the system is in a local energy minimum at this point in time). There is then a decrease in c-parameter to 20.0 Å (d_{002} = 10.0 Å), after which the system reaches an energy minimum. Furthermore, close inspection of the optimisation process suggests there is a brief point of inflection after around 100 optimisation cycles (Figure S6), with a c-parameter of 17.1 Å, possibly corresponding to the very short-lived intermediate noted in Figure 3(a).

It should be noted that there are small differences in the d-spacings observed experimentally and those calculated during the optimisation cycle. These can be attributed to differences in the amount of water in the model and in the interlayer in the real system (it is not possible to know the latter for all stages of the reaction), and also the fact that the chemical formula was simplified in the unconstrained model (Table 1 *cf.* Table 2) to ensure that simulations could be performed in a reasonable time period. However, these results strongly suggest that the intermediate observed is a result of the PAA ions first intercalating in a higher-energy orientation, before reorienting themselves to the most energetically favourable configuration. The sharp correlation between the MD and *in situ* results is striking, and to the best of our knowledge this is the first time that such observations have been reported. Our results suggest

1
2
3
4
5
6
7
8
9
10
11
12
13
14
15
16
17
18
19
20
21
22
23
24
25
26
27
28
29
30
31
32
33
34
35
36
37
38
39
40
41
42
43
44
45
46
47
48
49
50
51
52
53
54
55
56
57
58
59
60

that MD simulations may be used not only to model the final product, but that the energy minimisations which they use correspond closely to the molecular movements which take place in real reaction systems.

Intercalation of PAA$^-$

Data for the intercalation of PAA$^-$ into LiAl-Cl and LiAl-NO$_3$ are depicted in Figure 5. With both host materials, crystalline intermediate phases with lower d-spacings than the final product are observed in the diffraction data.
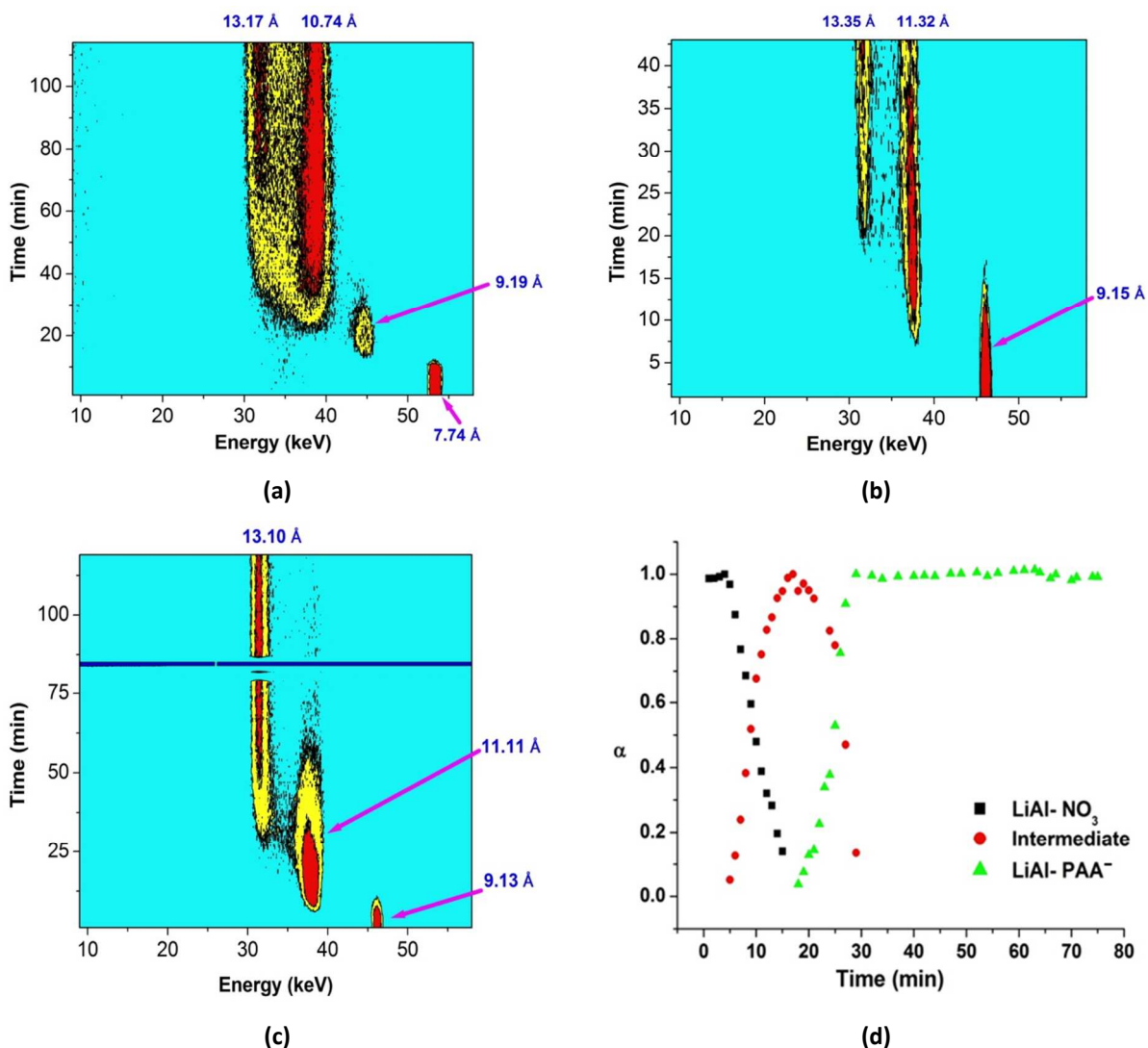
Figure 5: *In situ* XRD data obtained on DESY for the intercalation of PAA⁻. Contour plots of the raw data obtained at RT for **(a)** LiAl-Cl and **(b)** LiAl-NO₃; **(c)** raw data and **(d)** the extent of reaction *vs.* time plot for intercalation into LiAl-NO₃ at 70 °C. The blue line across the centre of the image in (c) arises owing to a temporary loss of the X-ray beam. An α vs time plot could not be constructed satisfactorily for intercalation into LiAl-Cl, owing to poor crystallinity of the phases, and thus is not included.

The intercalation of PAA⁻ into LiAl-Cl proceeds *via* two intermediate phases: initially the starting material at 7.74 Å can be seen, before a material with a reflection at 9.19 Å emerges, followed by a second at 10.74 Å, and then the final product at 13.17 Å. It should be noted that the latter is a significantly higher d-spacing that that observed *ex situ* for the final product. Complete conversion of the 10.74 Å phase to the 13.17 Å material is not observed during the timescale

over which the reaction was observed. The reaction product was recovered, filtered, and dried; XRD analysis of the resultant material showed it to have a d_{002} of *ca.* 11 Å. Therefore, the 13.17 Å phase observed *in situ* must be a highly hydrated material, which is converted to a material with an 11 Å interlayer spacing by drying.

In the case of LiAl-NO$_3$, in the room temperature reaction an initial reflection grows in at 11.32 Å, followed by the emergence of another reflection at around 13.4 Å. As in the LiAl-Cl case, both the 11.32 and 13.35 Å phases persist until reaction monitoring was ceased. To determine if the species around 11 Å is an intermediate or not, the reaction was repeated at 70 °C. At this elevated temperature, the 11 Å phase is clearly seen to grow in and then decline, leaving only a material with a d-spacing of 13.1 Å. The α *vs.* time curves for LiAl-NO$_3$ and the final product cross very close to zero, consistent with the presence of an intermediate. In contrast, the LiAl-NO$_3$/intermediate and intermediate/product sets of curves both cross at α = 0.5, showing that there are direct solid/solid transformations between these phases. The 70 °C reaction suspension was stored at RT for 24 h after monitoring ceased, and upon reanalysis d_{002} was shown to be 13.5 Å, The small increase in d-spacing over that observed during continuous monitoring can be ascribed to some additional hydration. As for LiAl-Cl, the final d-spacing observed *in situ* is higher than that observed *ex situ*. If the products are filtered and dried, then XRD shows the d-spacings of the dry products to be essentially the same as those prepared in the laboratory, indicating that the higher d-spacing phases are highly hydrated systems which are not stable to drying.

The reaction process for PAA$^-$ intercalation can thus be summarised as follows:

LiAl-Cl (7.74 Å) → Intermediate 1 (9.19 Å) → Intermediate 2 (10.74 Å) → Product (13.17 Å)

LiAl-NO$_3$ (9.15 Å) → Intermediate 2 (11.1 – 11.3 Å) → Product (13.1 – 13.35 Å)

The similarity of d-spacings for the 11 Å phase from both LiAl-Cl and LiAl-NO$_3$ indicates that they are probably the same material, with small differences in hydration. Given the fact that the first intermediate seen during PAA intercalation into LiAl-Cl has the same d-spacing as LiAl$_2$-NO$_3$, it

might be the case that this 9.19 Å phase also forms with the nitrate starting material, but cannot clearly be seen because the reflections overlap. As was the case with PAA^{3-}, the intermediates seen are not the result of staging (for LiAl-Cl, second and third stage intercalates with PAA$^-$ would have d_{004} of 9.4 and 13.3 Å; for LiAl-NO$_3$ 9.98 and 14.5 Å).

As for PAA^{3-}, MD simulations were performed for the LiAl-Cl starting material, and are presented in Figure 6. First, constrained simulations for PAA$^-$ were set up with one water molecule per Li$^+$ ion and the interlayer spacing observed for the dried *ex situ* product, and allowed to run until an energy minimum was reached. This reveals that in the final product observed *ex situ* the PAA$^-$ ions form a monolayer between the LDH layers, with a *d*-spacing of 10.91 ± 0.01 Å (Figure 6(a)). This is in good agreement with the *ex situ* experimental value of 11.1 Å, and the 10.74 Å observed *in situ*. The PAA$^-$ ions lie perpendicular across the interlayer regions (the detailed locations of the PAA$^-$ ions are given in Table S2).
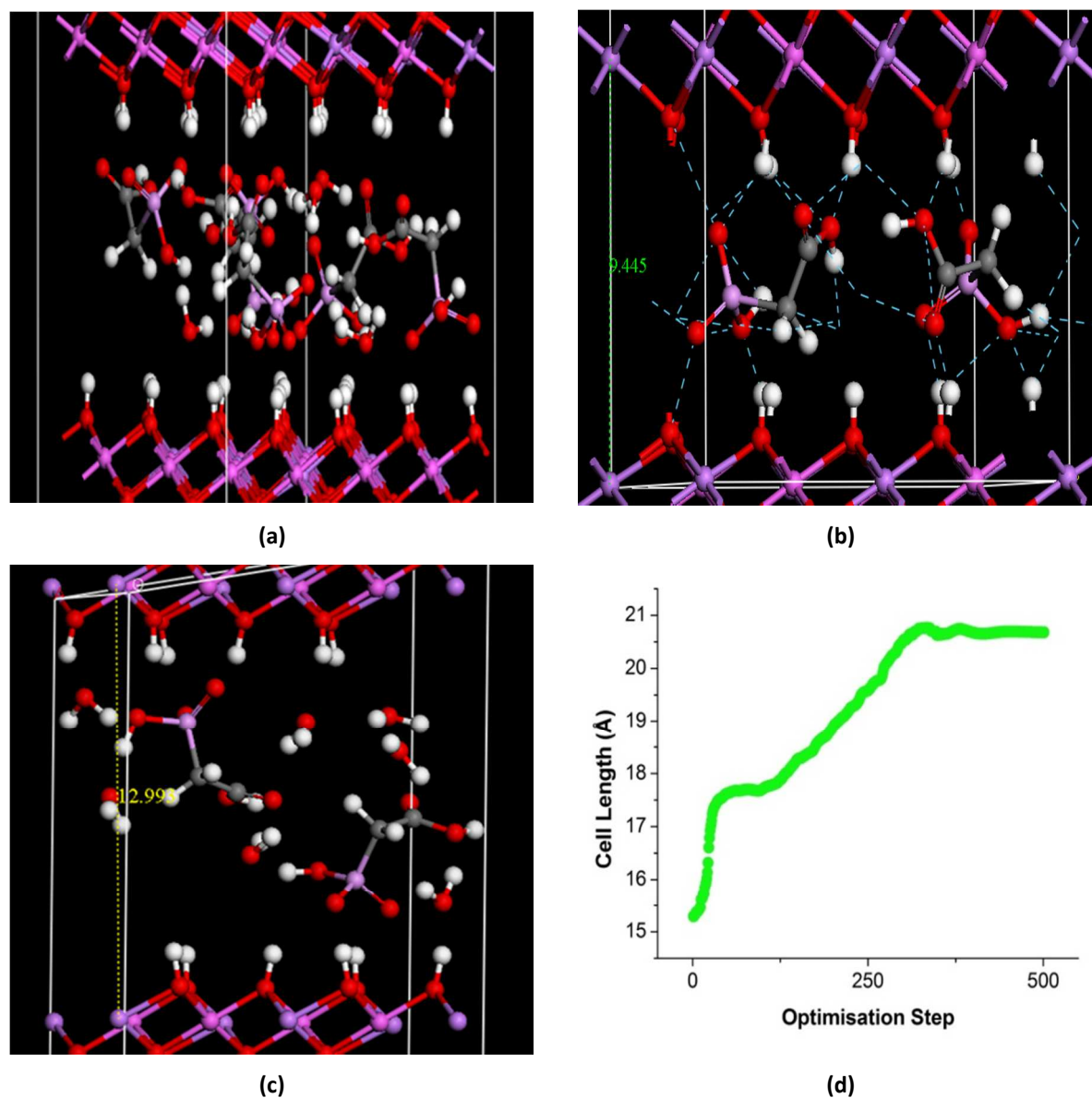
Figure 6: MD simulations for the intercalation of PAA⁻ into LiAl-Cl. **(a)** the energy minimised final product, **(b)** the orientation of PAA⁻ in the 9.2 Å intermediate phase, **(c)** the results of adding more water to the simulations, and, **(d)** the variation in cell c-parameter with optimisation cycle.

In the same way, we modelled the intermediate phase observed *in situ* at *ca.* 9.2 Å for LiAl-Cl (Figure 6(b)). This suggests that the PAA⁻ ions are intercalated in a horizontal manner in this system; they presumably re-orient later to give the final product. Additionally, further simulations were performed in which we increased the amount of water in the system, in order

to model the final, highly hydrated, material observed *in situ* at around 13 Å (see Figure 6(c)). When the simulations were rerun with six water molecules per unit cell, d_{002} is calculated to be 12.99 Å, in excellent agreement with the observed experimental value. The PAA⁻ ions are vertically oriented here, but the interlayer space is expanded because of the large amount of water present.

To understand in more detail the interlayer spacing evolution during the intercalation of PAA⁻, we again took the known structure for $[LiAl_2(OH)_6]Cl·H_2O$, deleted the Cl ions and manually inserted PAA⁻ between the layers (in the lowest energy orientation possible), and permitted the model to optimise without constraints. A plot of c-parameter *vs.* optimisation step is given in Figure 6(b); the c-parameter first increases rapidly to *ca.* 17.7 Å (d_{002} = 8.85 Å) before there is a plateau where despite further optimisation cycles running, no increase in c is seen. After around 125 cycles, the c-parameter again rises to 20.8 Å (d_{002} = 10.4 Å).

The d_{002} values calculated are a little different to those observed *in situ* (9.19 Å and 10.74 Å), for the same reasons as discussed above. However, the trend calculated by MD mirrors precisely what happens in the first stage of PAA⁻ intercalation *in situ*, with a lower d-spacing intermediate first forming and the d-spacing and then expanding. Re-running the model with varied amounts of water present (data not shown) led to changes in the absolute values of the d-spacings observed, but the variation of c-parameter with optimisation cycle follows the same trend in all cases – there is an initial rapid increase in c, followed by a plateau, and a second region of expansion before the model reaches an optimal configuration. The final product observed *in situ* at around 13 Å is not accounted for in the unconstrained model when the amount of water included is restricted to the amounts determined experimentally (see Table 1), but can be simulated when very large amounts of water are added to the unit cell in the model.

As for the intercalation of PAA³⁻, it is clear that MD simulations may be used not only to model the guest orientations in the final product, but also to understand the nanoscopic processes occurring along the reaction coordinate.

Intercalation of SAA

In situ data for the intercalation of SAA are given in Figure 7. Intercalation into both LiAl-Cl and LiAl-NO$_3$ proceed in an essentially identical fashion: the starting material declines in intensity before a phase grows in with d-spacing a little over 11 Å. There is then a distinct shift in the position of the latter reflection, to *ca.* 10.8 Å.
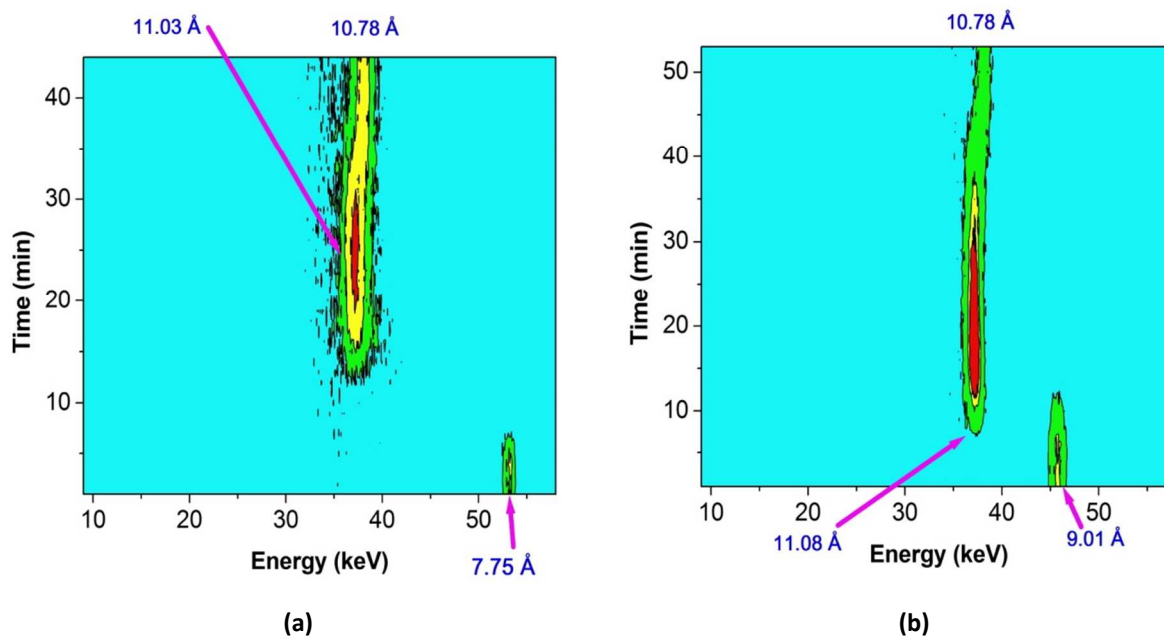

Figure 7: *In situ* XRD data for the intercalation of SAA into **(a)** LiAl-Cl and **(b)** LiAl-NO$_3$.

As was the case with PAA, the d-spacings of the phases observed are not consistent with staging, and MD simulations were performed to model the intercalation process into LiAl-Cl. The final energy minimised structure (calculated with constraints) showed SAA to form a monolayer in the interlayer space, with a d-spacing of 10.98 ± 0.01Å (Figure 8(a)). This is in good agreement with the *ex situ* experimental value of 10.5 Å, and the 10.78 Å seen *in situ*. The SAA ions lie perpendicular across the interlayer regions.
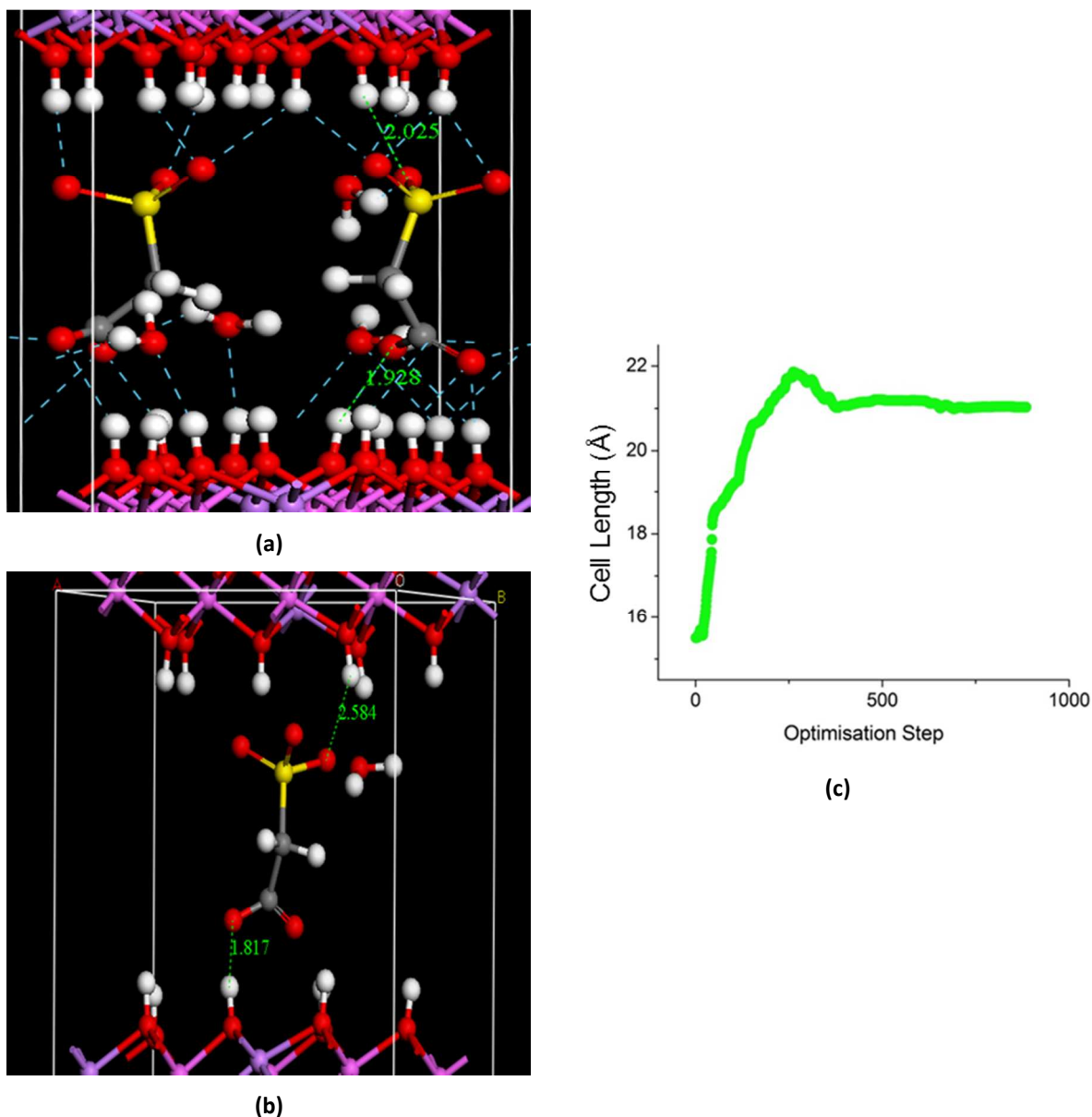
(a)

(b)

(c)

Figure 8: MD results for the intercalation of SAA into LiAl-Cl. **(a)** the proposed orientation of SAA in the interlayer space in the energy minimised system, **(b)** the orientation of SAA in the intermediate, and, **(c)** the change in the unit cell c-parameter with optimisation step.

The orientation of the SAA in the initial product with higher d-spacing was also modelled with constraints (Figure 8(b)), and looking at the guest orientations (see Figure 8(a) and (b)), the simulation study indicates that the SAA reorients itself after initial intercalation, presumably in order to maximise bonding interactions, and thus the initial d-spacing is higher than that observed at the end of the reaction.

Looking at the MD process run without constraints (Figure 8(c)), as increasing numbers of optimisation cycles are run, the simulation shows the c-parameter to rapidly increase to *ca.* 21.9 Å (d_{002} = 10.95 Å), which is very similar to the interlayer spacing of the initial material seen to form *in situ*. This subsequently declines to c = 21.1 Å (d_{002} = 10.6 Å) upon further optimisation cycles, again in excellent agreement with the reflection shift observed *in situ*. Beyond what is observed experimentally, the plot of cell length *vs.* optimisation cycle in Figure 8(b) includes a point of inflection at around 19 Å. This indicates that a very transient intermediate may exist, but the limitations of the *in situ* experiments do not allow this to be observed.

Intercalation of DPA

In situ data for DPA intercalation into LiAl-NO$_3$ are given in Figure 9. In these experiments, the pH of the DPA solution was adjusted to either 4.55 or 6.10 prior to the LDH being added.
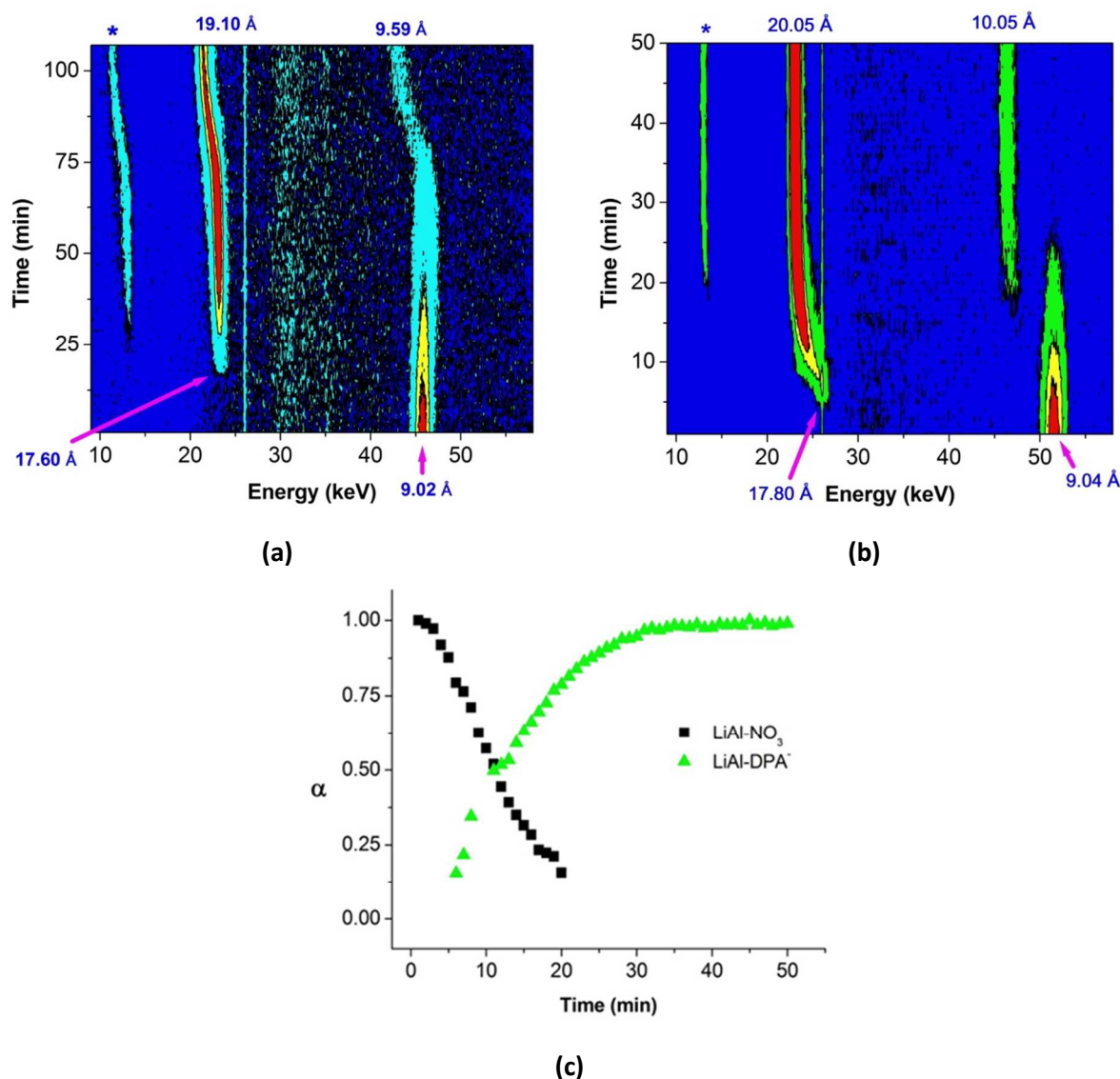
Figure 9: *In situ* XRD data collected on DESY for the intercalation of DPA into LiAl-NO$_3$ at **(a)** pH 4.55, and **(b)** pH 6.10; **(c)** the extend of reaction *vs.* time plot at pH 6.10. The reflections marked * in (a) and (b) are escape reflections from the detector.

No intermediates are observed for DPA intercalation: the starting material is converted directly to the product at both pH 4.55 and pH 6.10 (see Figure 9(a) and (b)). This is confirmed by the α *vs.* time curves in Figure 9(c); these cross at α = 0.5, confirming that there is no intermediate phase present here. However, there is a gradual increase in d$_{002}$ with time, from an initial 17.6 – 17.8 Å to 19.1 Å (pH 4.55) or 20.05 Å (pH 6.1). Similar shifts in position are seen in d$_{004}$.

Constrained MD simulations for DPA suggest the minimum energy structure is a bilayer arrangement with a *d*-spacing of 19.17 ± 0.02 Å (see Figure 10(a)). This is in reasonable agreement with the *ex situ* value of 18.6 Å, and a little lower that the final *in situ* d-spacings of 19 – 20 Å. The DPA anions are oriented in a perpendicular fashion across the interlayer regions, with their carboxylates facing the LDH layer and the ethylene chains towards the centre. The simulation shows that H-bonding occurs between the COO⁻ group of DPA and the LDH layer. The variation in cell length with optimisation step (Figure 10(b)), simulated using the unconstrained model, shows a very rapid increase in c-parameter to around 30.0 Å (d_{002} = 15.0 Å). This is followed by a more gradual increase in c, with the final c-value levelling off at *ca.* 36 Å (d_{002} = 18 Å). As for the previous systems studied, the unconstrained model mirrors very closely what is observed *in situ*, albeit with some differences between the interlayer spacings between the calculations and experimental observations. These may be ascribed to differences in hydration state.
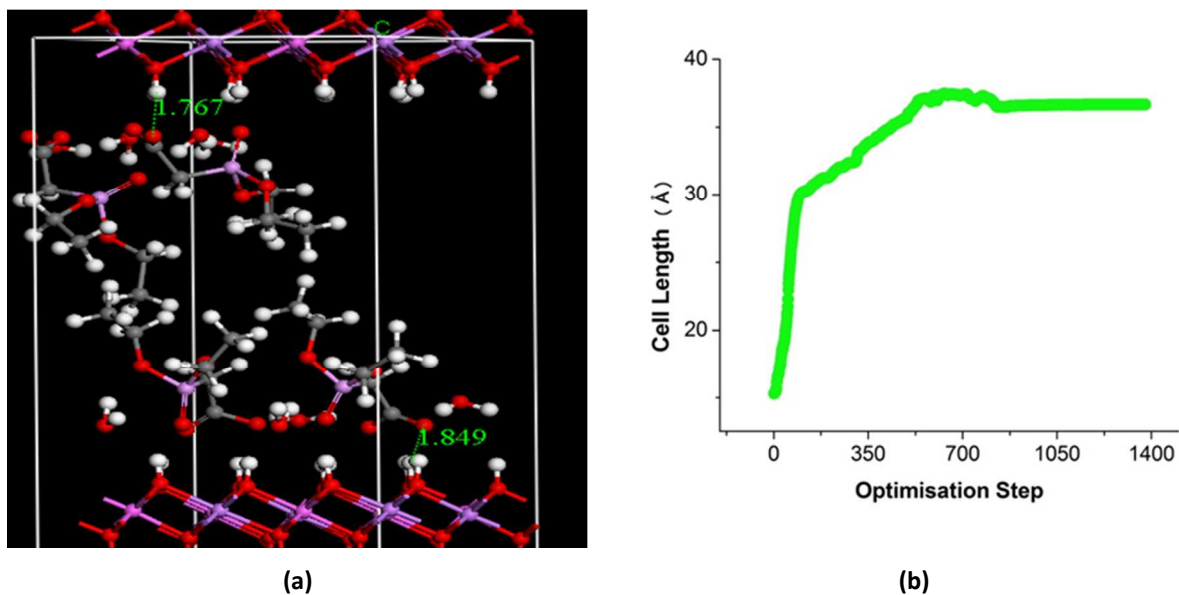

(a)   (b)

Figure 10: (a) the energy minimised structure of LiAl-DPA, and, **(b)** the variation of cell length with optimisation step.

Conclusions

A systematic study into the intercalation of the ions of phosphonoacetic acid (PAA), sulfoacetic acid (SAA) and diethylphosphonoacetic acid (DPA) into the layered double hydroxide (LDH) $[LiAl_2(OH)_6]X \cdot yH_2O$ (LiAl-X; X = Cl, NO_3) is reported. Three different anions of PAA, SAA^{2-} and DPA^- could easily be incorporated into the LDH. *In situ* time resolved X-ray diffraction experiments showed that the intercalation of PAA proceeds by very distinct intermediates, while shifts were observed in the interlayer spacing of the SAA and DPA intercalates as the reaction proceeded. The intermediate phases observed were distinct from simple staged systems. *In silico* molecular dynamics (MD) simulations were employed to gain more insight into the arrangement of ions in the interlayer space, and it was found that the different phases observed *in situ* correspond closely to local energy minima in the MD results. The results presented here demonstrate that MD simulations can be used not only to probe the orientation and interaction of guest species in host lattices, but also can unravel details of the intimate steps along the reaction coordinate.

Supporting information available

Additional XRD and IR data; an enlarged plot of variation in unit cell c-parameter with optimisation step for PAA^{3-} intercalation; the atom positions calculated in MD simulations. This material is available free of charge via the Internet at http://pubs.acs.org

References

(1)   *Layered Double Hydroxides*; Duan, X., Evans, D. G., Eds.; Structure and Bonding; Springer-Verlag: Berlin/Heidelberg, 2006; Vol. 119.

(2)   Fogg, A. M.; Freij, A.J.; Parkinson, G.M. Synthesis and Anion Exchange Chemistry of Rhombohedral Li/Al Layered Double Hydroxides. *Chem. Mater.* **2002**, *14*, 232-234

(3)   Wang, Z.; Han, E.; Ke, W. Influence of Nano-LDHs on Char Formation and Fire-Resistant Properties of Flame-Retardant Coating. *Prog. Org. Coatings* **2005**, *53*, 29–37.

(4)   Kagunya, W.; Hassan, Z.; Jones, W. Catalytic Properties of Layered Double Hydroxides and Their Calcined Derivatives. *Inorg. Chem.* **1996**, *35*, 5970–5974.

(5)   Gong, M.; Li, Y.; Wang, H.; Liang, Y.; Wu, J. Z.; Zhou, J.; Wang, J.; Regier, T.; Wei, F.; Dai, H. An Advanced Ni-Fe Layered Double Hydroxide Electrocatalyst for Water Oxidation. *J. Am. Chem. Soc.* **2013**, *135*, 8452–8455.

(6)   He, S.; An, Z.; Wei, M.; Evans, D. G.; Duan, X. Layered Double Hydroxide-Based Catalysts: Nanostructure Design and Catalytic Performance. *Chem. Commun.* **2013**, *49*, 5912–5920.

(7)   Theiss, F. L.; Sear-Hall, M. J.; Palmer, S. J.; Frost, R. L. Zinc Aluminium Layered Double Hydroxides for the Removal of Iodine and Iodide from Aqueous Solutions. *Desalin. Water Treat.* **2012**, *39*, 166–175.

(8)   Jin, S.; Bland, A. E.; Brown, T. H. Bioagent Air Filtration Systems. CA2513469 A1, 2005.

(9)   Dutta, P. K.; Robins, D. S. Pyrene Sorption in Organic-Layered Double-Metal Hydroxides. *Langmuir* **1994**, *10*, 1851–1856.

(10)   Monash, P.; Pugazhenthi, G. Utilization of Calcined Ni-Al Layered Double Hydroxide (LDH) as an Adsorbent for Removal of Methyl Orange Dye from Aqueous Solution. *Environ. Prog. Sustain. Energy* **2014**, *33*, 154–159.

(11)   Bruna, F.; Celis, R.; Pavlovic, I.; Barriga, C.; Cornejo, J.; Ulibarri, M. A. Layered Double Hydroxides as Adsorbents and Carriers of the Herbicide (4-Chloro-2-

Methylphenoxy)acetic Acid (MCPA): Systems Mg-Al, Mg-Fe and Mg-Al-Fe. *J. Hazard. Mater.* **2009**, *168*, 1476–1481.

(12)   Ogawa, M.; Kuroda, K. Photofunctions of Intercalation Compounds. *Chem. Rev.* **1995**, *95*, 399–438.

(13)   Millange, F.; Walton, R. I.; Lei, L.; O'Hare, D. Efficient Separation of Terephthalate and Phthalate Anions by Selective Ion-Exchange Intercalation in the Layered Double Hydroxide $Ca_2Al(OH)_6 \cdot NO_3 \cdot 2H_2O$. *Chem. Mater.* **2000**, *12*, 1990–1994.

(14)   Ragavan, A.; Khan, A. I.; O'Hare, D. Isomer Selective Ion-Exchange Intercalation of Nitrophenolates into the Layered Double Hydroxide $[LiAl_2(OH)_6]Cl \cdot xH_2O$. *J. Mater. Chem.* **2006**, *16*, 602.

(15)   Khan, A. I.; Lei, L.; Norquist, A. J.; O'Hare, D. Intercalation and Controlled Release of Pharmaceutically Active Compounds from a Layered Double Hydroxide. *Chem. Commun.* **2001**, 2342–2343.

(16)   Yang, J.; Han, Y.; Park, M.; Park, T.; Hwang, S.; Choy, J. New Inorganic-Based Drug Delivery System of Indole-3-Acetic Acid-Layered Metal Hydroxide Nanohybrids with Controlled Release Rate. *Chem. Mater.* **2007**, *19*, 2679–2685.

(17)   Ambrogi, V.; Fardella, G.; Grandolini, G.; Perioli, L. Intercalation Compounds of Hydrotalcite-like Anionic Clays with Antiinflammatory Agents--I. Intercalation and in Vitro Release of Ibuprofen. *Int. J. Pharm.* **2001**, *220*, 23–32.

(18)   Williams, G. R.; Moorhouse, S. J.; Prior, T. J.; Fogg, A. M.; Rees, N. H.; O'Hare, D. New Insights into the Intercalation Chemistry of $Al(OH)_3$. *Dalton Trans.* **2011**, *40*, 6012–6022.

(19)   Khan, A. I.; Williams, G. R.; Hu, G.; Rees, N. H.; O'Hare, D. The Intercalation of Bicyclic and Tricyclic Carboxylates into Layered Double Hydroxides. *J. Solid State Chem.* **2010**, *183*, 2877–2885.

(20)   Wei, M.; Pu, M.; Guo, J.; Han, J.; Li, F.; He, J.; Evans, D. G.; Duan, X. Intercalation of L - Dopa into Layered Double Hydroxides: Enhancement of Both Chemical and Stereochemical Stabilities of a Drug through Host–Guest Interactions. *Chem. Mater.* **2008**, *20*, 5169–5180.

(21)   Markland, C.; Williams, G. R.; O'Hare, D. The Intercalation of Flavouring Compounds into Layered Double Hydroxides. *J. Mater. Chem.* **2011**, *21*, 17896.

(22)   Williams, G. R.; Rees, N. H.; O'Hare, D. Incorporation of Phosphorus Oxyacids into Layered Double Hydroxides. *Solid State Sci.* **2009**, *11*, 1229–1238.

(23)   Jellicoe, T. C.; Fogg, A. M. Synthesis and Characterization of Layered Double Hydroxides Intercalated with Sugar Phosphates. *J. Phys. Chem. Solids* **2012**, *73*, 1496–1499.

(24)   Williams, G. R.; Norquist, A. J.; O'Hare, D. Time-Resolved, In Situ X-Ray Diffraction Studies of Staging during Phosphonic Acid Intercalation into $[LiAl_2(OH)_6]Cl\cdot H_2O$. *Chem. Mater.* **2004**, *16*, 975–981.

(25)   Williams, G. R.; O'Hare, D. New Phosphonate Intercalates of $[Ca_2Al(OH)_6]NO_3\cdot yH_2O$: A Synthetic and Kinetic Study. *Solid State Sci.* **2006**, *8*, 971–980.

(26)   Williams, G. R.; Fogg, A. M.; Sloan, J.; Taviot-Guého, C.; O'Hare, D. Staging during Anion-Exchange Intercalation into $[LiAl_2(OH)_6]Cl\cdot yH_2O$: Structural and Mechanistic Insights. *Dalton Trans.* **2007**, *2*, 3499–3506.

(27)   Auxilio, A. R.; Andrews, P. C.; Junk, P. C.; Spiccia, L.; Neumann, D.; Raverty, W.; Vanderhoek, N. Adsorption and Intercalation of Acid Blue 9 on Mg–Al Layered Double Hydroxides of Variable Metal Composition. *Polyhedron* **2007**, *26*, 3479–3490.

(28)   Costa, F. R.; Leuteritz, A.; Wagenknecht, U.; Auf der Landwehr, M.; Jehnichen, D.; Haeussler, L.; Heinrich, G. Alkyl Sulfonate Modified LDH: Effect of Alkyl Chain Length on Intercalation Behavior, Particle Morphology and Thermal Stability. *Appl. Clay Sci.* **2009**, *44*, 7–14.

(29)   Oriakhi, C. O.; Farr, I. V; Lerner, M. M. Thermal Characterization of Poly(styrene Sulfonate) Layered Double Hydroxide Nanocomposites. *Clays Clay Miner.* **1997**, *45*, 194–202.

(30)   Williams, G. R.; Khan, A. I.; O'Hare, D. Mechanistic and Kinetic Studies of Guest Ion Intercalation into Layered Double Hydroxides Using Time-Resolved, in-Situ X-Ray Power Diffraction. *Struct. Bond.* **2005**, *119*, 161–192.

(31)   Williams, G. R.; Norquist, A. J.; O'Hare, D. The Formation of Ordered Heterostructures during the Intercalation of Phosphonic Acids into a Layered Double Hydroxide. *Chem. Commun.* **2003**, 1816.

(32)   Fogg, A. M.; Dunn, J. S.; O'Hare, D. Formation of Second-Stage Intermediates in Anion-Exchange Intercalation Reactions of the Layered Double Hydroxide $[LiAl_2(OH)_6]Cl\cdot H_2O$ as Observed by Time-Resolved, in Situ X-Ray Diffraction. *Chem. Mater.* **1998**, *10*, 356–360.

(33)   Williams, G. R.; O'Hare, D. Factors Influencing Staging during Anion-Exchange Intercalation into $[LiAl_2(OH)_6]X\cdot mH_2O$ (X = Cl^-, Br^-, NO_3^-). *Chem. Mater.* **2005**, *17*, 2632–2640.

(34)   Feng, Y. J.; Williams, G. R.; Leroux, F.; Taviot-Gueho, C.; O'Hare, D. Selective Anion-Exchange Properties of Second-Stage Layered Double Hydroxide Heterostructures. *Chem. Mater.* **2006**, *18*, 4312–4318.

(35)   Newman, S. P.; Di Cristina, T.; Coveney, P. V.; Jones, W. Molecular Dynamics Simulation of Cationic and Anionic Clays Containing Amino Acids. *Langmuir* **2002**, *18*, 2933–2939.

(36)   Yan, D.; Lu, J.; Wei, M.; Evans, D. G.; Duan, X. Recent Advances in Photofunctional Guest/layered Double Hydroxide Host Composite Systems and Their Applications: Experimental and Theoretical Perspectives. *J. Mater. Chem.* **2011**, *21*, 13128.

(37)   Gao, R.; Zhao, M.; Guan, Y.; Fang, X.; Li, X.; Yan, D. Ordered and Flexible Lanthanide Complex Thin Films Showing up-Conversion and Color-Tunable Luminescence. *J. Mater. Chem. C* **2014**, *2*, 9579–9586.

(38)   Yan, D.; Lu, J.; Wei, M.; Ma, J.; Evans, D. G.; Duan, X. A Combined Study Based on Experiment and Molecular Dynamics: Perylene Tetracarboxylate Intercalated in a Layered Double Hydroxide Matrix. *Phys. Chem. Chem. Phys.* **2009**, *11*, 9200–9209.

(39)   Yan, D.; Lu, J.; Ma, J.; Wei, M.; Li, S.; Evans, D. G.; Duan, X. Near-Infrared Absorption and Polarized Luminescent Ultrathin Films Based on Sulfonated Cyanines and Layered Double Hydroxide. *J. Phys. Chem. C* **2011**, *115*, 7939–7946.

(40)   Zhao, Y.; Lin, H.; Chen, M.; Yan, D. Niflumic Anion Intercalated Layered Double Hydroxides with Mechano-Induced and Solvent-Responsive Luminescence. *Ind. Eng. Chem. Res.* **2014**, *53*, 3140–3147.

(41)   Thyveetil, M. A.; Coveney, P. V; Greenwell, H. C.; Suter, J. L. Role of Host Layer Flexibility in DNA Guest Intercalation Revealed by Computer Simulation of Layered Nanomaterials. *J. Am. Chem. Soc.* **2008**, *130*, 12485–12495.

(42)   Thyveetil, M.; Coveney, P. V; Greenwell, H. C.; Suter, J. L. Computer Simulation Study of the Structural Stability and Materials Properties of DNA-Intercalated Layered Double Hydroxides. *J. Am. Chem. Soc.* **2008**, *130*, 4742–4756.

(43)   Besserguenev, A. V; Fogg, A. M.; Francis, R. J.; Price, S. J.; O'Hare, D.; Isupov, V. P.; Tolochko, B. P. Synthesis and Structure of the Gibbsite Intercalation Compounds $[LiAl_2(OH)_6]X$ {X = Cl, Br, NO_3} and $[LiAl_2(OH)_6]Cl \cdot H_2O$ Using Synchrotron X-Ray and Neutron Powder Diffraction. *Chem. Mater.* **1997**, *9*, 241–247.

(44)   Moorhouse, S. J.; Vranješ, N.; Jupe, A.; Drakopoulos, M.; O'Hare, D. The Oxford-Diamond In Situ Cell for Studying Chemical Reactions Using Time-Resolved X-Ray Diffraction. *Rev. Sci. Instrum.* **2012**, *83*, 084101.

(45)   Hammersley, A. P. FIT2D V9.129 Reference Manual V123.121, 1998.

(46)   Avrami, M. Granulation, Phase Change, and Microstructure Kinetics of Phase Change. III. *J. Chem. Phys.* **1941**, *9* (2), 177.

(47)   Avrami, M. Kinetics of Phase Change. I General Theory. *J. Chem. Phys.* **1939**, *7*, 1103.

(48)   Avrami, M. Kinetics of Phase Change. II Transformation-Time Relations for Random Distribution of Nuclei. *J. Chem. Phys.* **1940**, *8*, 212.

(49)   Erofe'ev, B. Generalized Equation of Chemical Kinetics and Its Application in Reactions Involving Solids. *Compt Rend Acad Sci USSR* **1946**, *52*, 511–514.

(50)   Zhang, S. T.; Yan, H.; Wei, M.; Evans, D. G.; Duan, X. Valence Force Field for Layered Double Hydroxide Materials Based on the Parameterization of Octahedrally Coordinated Metal Cations. *J. Phys. Chem. C* **2012**, *116*, 3421–3431.

(51)   Andersen, H. C. Molecular Dynamics Simulations at Constant Pressure And/or Temperature. *J. Chem. Phys.* **1980**, *72*, 2384.

(52)   Berendsen, H. J. C.; Postma, J. P. M.; van Gunsteren, W. F.; DiNola, A.; Haak, J. R. Molecular Dynamics with Coupling to an External Bath. *J. Chem. Phys.* **1984**, *81*, 3684–3690.

(53)   Allen, M.; Tildesley, D. *Computer Simulation of Liquids*; Clarendon Press: Oxford, 1987.

(54)   Casalini, T.; Salvalaglio, M.; Perale, G.; Masi, M.; Cavallotti, C. Diffusion and Aggregation of Sodium Fluorescein in Aqueous Solutions. *J. Phys. Chem. B* **2011**, *115*, 12896–12904.

(55)   Accelrys Software Inc. Materials Studio 5.5. *San Diego, USA*, 2010.

(56)   ChemAxon. Marvin 6.0.1, 2013.

(57)   Mohanambe, L.; Vasudevan, S. Anionic Clays Containing Anti-Inflammatory Drug Molecules: Comparison of Molecular Dynamics Simulation and Measurements. *J. Phys. Chem. B* **2005**, *109*, 15651–15658.

(58)   Greenwell, H. C.; Harvey, M. J.; Boulet, P.; Bowden, A. a.; Coveney, P. V.; Whiting, A. Interlayer Structure and Bonding in Nonswelling Primary Amine Intercalated Clays. *Macromolecules* **2005**, *38*, 6189–6200.

(59)   Wang, J.; Kalinichev, A. G.; Kirkpatrick, R. J. Effects of Substrate Structure and Composition on the Structure, Dynamics, and Energetics of Water at Mineral Surfaces: A Molecular Dynamics Modeling Study. *Geochim. Cosmochim. Acta* **2006**, *70*, 562–582.

(60)   Xu, S.-M.; Zhang, S.-T.; Shi, W.-Y.; Ning, F.-Y.; Fu, Y.; Yan, H. Understanding the Thermal Motion of the Luminescent Dyes in the Dye–surfactant Cointercalated ZnAl-Layered Double Hydroxides: A Molecular Dynamics Study. *RSC Adv.* **2014**, *4*, 47472–47480.

Combined *In Situ* and *In Silico* Studies of Guest Intercalation into the Layered Double Hydroxide [LiAl$_2$(OH)$_6$]X·yH$_2$O

TOC image